Asociación Argentina
de Mecánica Computacional

Mecánica Computacional Vol XXVI, pp.2943-2958
Sergio A. Elaskar, Elvio A. Pilotta, Germán A. Torres (Eds.)
Córdoba, Argentina, Octubre 2007

DYNAMICS OF MULTIBODY SYSTEMS WITH BOND GRAPHS

Germán Filippini, Diego Delarmelina, Jorge Pagano, Juan Pablo Alianak, Sergio Junco and Norberto Nigro

Facultad de Ciencias Exactas, Ingeniería y Agrimensura
Universidad Nacional de Rosario, Av. Pellegrini 250, S2000EKE Rosario, Argentina.

Keywords: Bond Graphs, Multibody systems.

Abstract. In this work a general multibody system theory is implemented within a bond graph modeling framework. In classical mechanics several procedures exist by which differential equations can be derived of a system of rigid bodies. In the case of large systems these procedures are labor-intensive and consequently error-prone, unless they are computerized. The bond graphs formalism allows for a unified modeling of multidisciplinary physical systems. It is well-suited for a modular modeling approach based on physical principles. The theory of multibody system dynamics in terms of bond graphs modeling is revisited with the purpose of designing a multibond graph library for such systems. Several mechanical systems undergoing large 3-dimensional rotations are numerically solved in order to validate this software library written in 20-sim software.

1 INTRODUCTION

Modeling and simulation has an increasing importance in the development of complex, large mechanical systems. In areas like road vehicles (Bos (1986); Filippini (2004); Filippini et al. (2007)), rail vehicles, high speed mechanisms, industrial robots and machine tools (Ersal (2004)), simulation is an inexpensive way to experiment with the system and to design an appropriate control system.

The above indicated kind of mechanical systems belong to a broader class of rigid body systems frequently called multibody systems. They consist of a finite number of rigid bodies, interconnected by arbitrary joints. The latter may exhibit properties of rotational or translational degrees of freedom, also damping and compliance, and normally contain some sort of attachment for drives and external forces.

In classical mechanics several procedures exist through which differential equations can be derived for a system of rigid bodies. In the case of large systems these procedures are labor-intensive and consequently error-prone, unless they are computerized (Shabana; Geradin-Cardona 2001).

This work applies the multibody theory through the multibond or vector bond graph technique (Rosenberg; Bos (1986); Cellier; Ersal (2004)) with the purpose of designing a multibond graph library for such system. Primarily, bond graphs represent elementary energy-related phenomena (generation, storage, dissipation, power exchange) using a small set of ideal elements that can be coupled together through external ports representing power flow. Thus, they are well-suited for a modular modeling approach based on physical principles. Hierarchical modeling becomes possible through coupling of component or subsystems models through their connecting ports. Besides these physical features capturing energy exchange phenomena, it is also possible to code on the graph the mathematical structure of the physical system, in the sense of showing the causal relationships (in a computational sense) among its signals. On the one side, this allows connecting BG-models to signal flow graphs or block diagrams, and -on the other side- it turns the algorithmic derivation of mathematical and computational models from BG into a highly formalized task (Rosenberg). The conjunction of all these features make of BG a physically based, object-oriented graphical language most suitable for dynamic modeling, analysis and simulation of complex engineering systems involving mixed physical and technical domains in their constitution (Cellier).

2 MATHEMATICAL AND BG MODELING

This section presents the multibond graph library and addresses the essential issues concerning the bond graph modeling of multibody systems as used in this work.

2.1 Rigid Body

To determine the spatial motion of the rigid body the well known Euler equations are used, which appear in (1) and (2) in both, their intrinsic way of representation and their tensorial counterparts.

The first one represents the conservation of linear momentum, written as:

$$\sum \bar{F} = \frac{d\bar{p}}{dt} = \left.\frac{d\bar{p}}{dt}\right|_{rel} + \bar{\omega} \times \bar{p}$$
$$F_i = \frac{dp_i}{dt} = \left.\frac{dp_i}{dt}\right|_{rel} + \varepsilon_{ijk}\omega_j p_k \tag{1}$$

where $\bar{F}, \bar{\omega}, \bar{p}$ represents the external forces, the angular velocity vector and the linear momentum vector respectively; *d/dt, d/dt|rel,* ε_{ijk} represent the derivative respect to the inertial frame, the derivative respect to the body attached frame and the Levi-Civita tensor used to express the cross product in tensor notation.

The second of the Euler equations sets up the conservation of angular momentum:

$$\sum \bar{M} = \frac{d\bar{h}}{dt} = \left.\frac{d\bar{h}}{dt}\right|_{rel} + \bar{\omega} \times \bar{h}$$
$$M_i = \frac{dh_i}{dt} = \left.\frac{dh_i}{dt}\right|_{rel} + \varepsilon_{ijk}\omega_j h_k \tag{2}$$

where $\bar{M}$, $\bar{h}$ represent the external torque and the angular momentum vector.

The bond graph representation of the 3-dimensional motion of a rigid body based on the Euler equations is shown in figure 1. Three power multibonds are attached to the upper **1**-junction representing the center-of-mass speed-vector $\bar{v}$. The effort variable associated to the multibond pointing into the inertia **I**:m is the first term in the right-hand side of (1); the effort of the multibond on the left is the second term of the right-hand side, while that of the multibond on the right is the term of the left-hand side. The latter represents the external forces acting on the center-of-mass point of the body and, thus, it is an input or external connection port of this module. An analog description can be given for the lower **1**-junction concerning the rotational speed vector $\bar{\omega}$ and the torques in (2). Note the multisignal link from the lower **1**-junction to the **MGR**-element, necessary to implement the modulation of the second term in the right-hand side of (1) by the speed $\bar{\omega}$. The components of the inertia matrix $\bar{J}$ are the principal moments of inertia with respect to the principal axes of the rigid body. The lower part of Fig. 1 is the mask which will be used as a compact representation when connecting this model to others in the case of modeling a complex system.

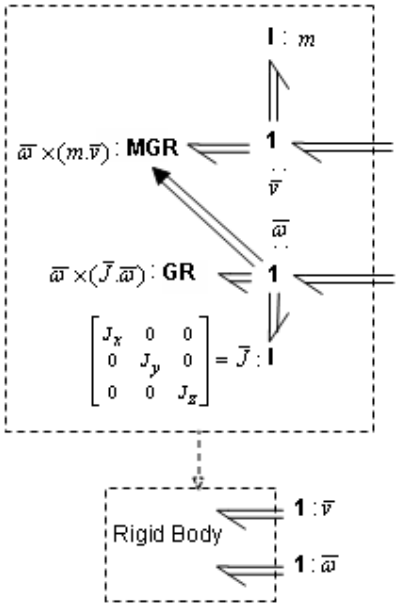

Fig. 1: Bond Graphs representation of the spatial rigid body dynamics.

2.2 Transformation of Translation

The port variables of the above model are defined respect to the system attached to the center of mass of the rigid body. Referring these port variables to the coordinates of interconnection with other bodies allow to couple the whole model. Figure 2 shows the bond graph implementation of the equation system representing how the port variables of two arbitrary points 'A' and 'B' of a given spatial body transform each other. The equations relating the linear and rotational efforts are the following:

$$\begin{aligned} \overline{M} &= \overline{F} \times \overline{r} \\ M_i &= \varepsilon_{ijk} F_j r_k \end{aligned} \tag{3}$$

For the flow variables the equations are the following:

$$\begin{aligned} \overline{v} &= \overline{\omega} \times \overline{r} \\ v_i &= \varepsilon_{ijk} \omega_j r_k \end{aligned} \tag{4}$$

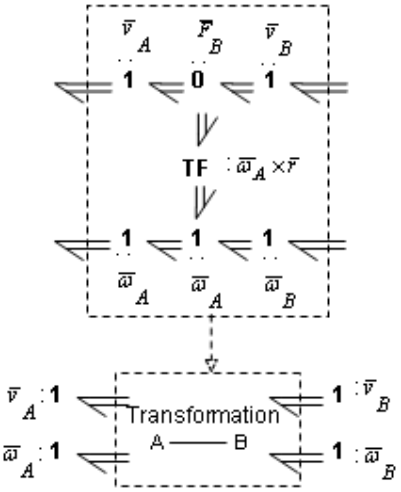

Fig. 2: Power variables transformation between two points 'A', 'B' belonging to a given 3-dimensional rigid body.

2.3 Transformation of Rotation

To transform the dynamic equations from those expressed in the body attached frame of reference (roll, pitch and yaw axes) to a spatially fixed frame of reference (X,Y,Z : inertial frame) it is necessary to choose some parameterization for the rotations. Among the multiple possibilities, Euler angles are used in this work. To transform these rotations the following equations are used:

$$\bar{\omega}'' = \bar{\phi}\,\bar{\omega} \quad (5.a); \qquad \bar{\omega}' = \bar{\theta}\,\bar{\omega}'' \quad (5.b); \qquad \bar{\omega}^G = \bar{\psi}\,\bar{\omega}' \quad (5.c)$$

$$\bar{v}'' = \bar{\phi}\,\bar{v} \quad (5.d); \qquad \bar{v}' = \bar{\theta}\,\bar{v}'' \quad (5.e); \qquad \bar{v}^G = \bar{\psi}\,\bar{v}' \quad (5.f)$$

where,

$$\bar{\phi} = \begin{bmatrix} 1 & 0 & 0 \\ 0 & \cos\phi & -\sin\phi \\ 0 & \sin\phi & \cos\phi \end{bmatrix} \quad \bar{\theta} = \begin{bmatrix} \cos\theta & 0 & \sin\theta \\ 0 & 1 & 0 \\ -\sin\theta & 0 & \cos\theta \end{bmatrix} \quad \bar{\psi} = \begin{bmatrix} \cos\psi & -\sin\psi & 0 \\ \sin\psi & \cos\psi & 0 \\ 0 & 0 & 1 \end{bmatrix}$$

$$\bar{\omega} = \begin{bmatrix} \omega_x \\ \omega_y \\ \omega_z \end{bmatrix} \quad \bar{\omega}'' = \begin{bmatrix} \omega_x'' \\ \omega_y'' \\ \omega_z'' \end{bmatrix} \quad \bar{\omega}' = \begin{bmatrix} \omega_x' \\ \omega_y' \\ \omega_z' \end{bmatrix} \quad \bar{\omega}^G = \begin{bmatrix} \omega_X \\ \omega_Y \\ \omega_Z \end{bmatrix}$$

$$\bar{v} = \begin{bmatrix} v_x \\ v_y \\ v_z \end{bmatrix} \quad \bar{v}'' = \begin{bmatrix} v_x'' \\ v_y'' \\ v_z'' \end{bmatrix} \quad \bar{v}' = \begin{bmatrix} v_x' \\ v_y' \\ v_z' \end{bmatrix} \quad \bar{v}^G = \begin{bmatrix} v_X \\ v_Y \\ v_Z \end{bmatrix}$$

Its bond graphs representation is observed in figure 3, where the power variables are transformed from (x,y,z) axes to the rotated ones (X,Y,Z) according to the angles ϕ, θ, ψ respect to each axis. It may be observed that while the flow variables are rotated from (xyz) to

(XYZ), the effort variables are transformed back from (XYZ) to (xyz).

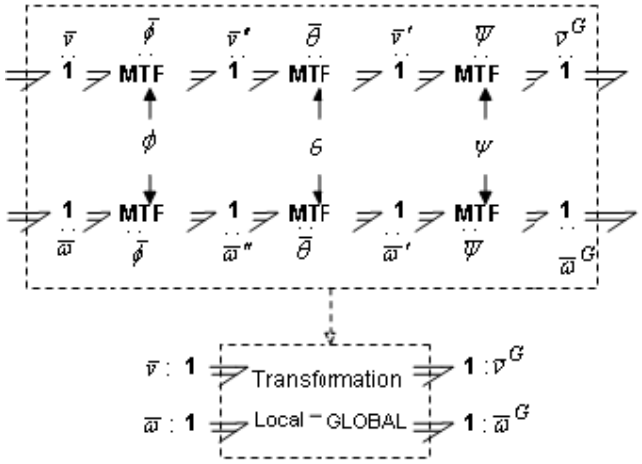

Fig. 3: 3-dimensional rotation equations expressed in terms of power variables.

2.4 Spherical Joint

The Spherical Joint element is a joint that allows three main axis rotations between the joined bodies. It means, translation freedom is restricted on the three frame axes, meanwhile the rotation is not.

The bond graph representation of the Spherical Joint is shown in figure 4. **Se**=0 is a null effort source that does not impose any torque at both joint ends. The $\overline{v}_1^J = \overline{v}_2^J$ relationship is achieved through the use of **C** elements with specific parameters values, making the joint flexible instead of completely rigid. It is important to note that vectors $\overline{v}_1$ and $\overline{v}_2$, shown in Fig. 4, may not be equal; in fact these vectors represent the joint connected rigid body velocities respect to the self local frame. Vector projections $\overline{v}_1$ and $\overline{v}_2$ at joint reference frame, made by a modular transformation tool, allows the joint to calculate efforts at this frame system. At the same time, by the same transformation, the calculated efforts at joint reference frame may be projected to the local reference frame of each body.

Modular transformation is obtained with the matrices shown in 2.3, which depend on the angles between each self body attached local frame to the local frame of the joint. For this kind of joint the following transformations are required:

$$\begin{bmatrix} v_x^J \\ v_y^J \\ v_z^J \end{bmatrix} = \overline{\psi}\overline{\theta}\overline{\phi} \begin{bmatrix} v_x \\ v_y \\ v_z \end{bmatrix} \quad ; \quad \begin{bmatrix} F_x \\ F_y \\ F_z \end{bmatrix} = (\overline{\psi}\overline{\theta}\overline{\phi})^t \begin{bmatrix} F_x^J \\ F_y^J \\ F_z^J \end{bmatrix}$$

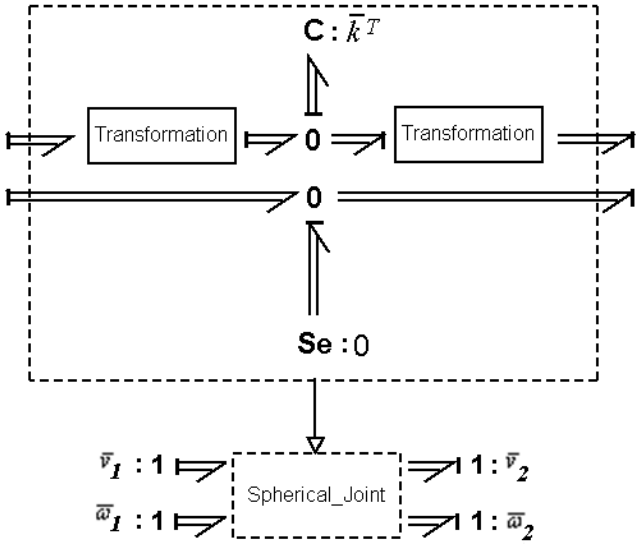

Fig. 4: Bond Graphs representation of the Spherical Joint.

2.5 Revolute Joint

The Revolute Joint element is a joint that allows turning the bodies joined between them. Therefore, three translations and two rotational degrees of freedom are constrained, leaving only one rotation degree of freedom free.

The bond graph representation of the Revolute Joint is shown in figure 5. At the RJ (Revolute Joint) like as SJ (Spherical joint), constrains are controllable by the use of **C** elements. The $\bar{k}^T$ parameter must be accurate enough to obtain approximately $\bar{v}_1^J = \bar{v}_2^J$. Fig. 5 shows two **C** elements with parameters k^{Ry} and k^{Rz} that allow to obtain $\omega_{1y}^J = \omega_{2y}^J$ and $\omega_{1z}^J = \omega_{2z}^J$, the same constraint for the rotational fixations.

Therefore, this kind of joint has only one degree of freedom. The **Se**=0 null effort source does not impose any x-axis torque at both joint ends.

Due to this joint condition, only one angle changes between those connected bodies, the modular transformation associated may be solved with only one of the matrices in 2.3 i.e. if rotation axis is x (as in this case), then only matrix $\bar{\phi}$ (defined above) has to be used.

$$\begin{bmatrix} v_x^J \\ v_y^J \\ v_z^J \end{bmatrix} = \bar{\phi} \begin{bmatrix} v_x \\ v_y \\ v_z \end{bmatrix} \quad ; \quad \begin{bmatrix} F_x \\ F_y \\ F_z \end{bmatrix} = (\bar{\phi})^t \begin{bmatrix} F_x^J \\ F_y^J \\ F_z^J \end{bmatrix}$$

$$\begin{bmatrix} \omega_x^J \\ \omega_y^J \\ \omega_z^J \end{bmatrix} = \bar{\phi} \begin{bmatrix} \omega_x \\ \omega_y \\ \omega_z \end{bmatrix} \quad ; \quad \begin{bmatrix} M_x \\ M_y \\ M_z \end{bmatrix} = (\bar{\phi})^t \begin{bmatrix} M_x^J \\ M_y^J \\ M_z^J \end{bmatrix}$$

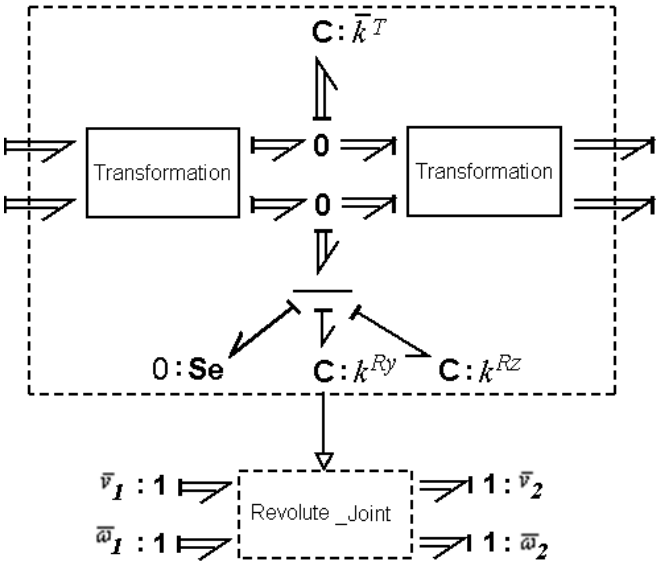

Fig. 5: Bond Graphs representation of the Revolute Joint.

2.6 Prismatic Joint

The Prismatic Joint (PJ) is a joint that allow only a straight displacement between its joined bodies, fixing the remaining two translational and the whole three rotational degrees of freedom. Therefore, only one generalized coordinate is free to change.

Figure 6 shows the bond graph implementation of the Prismatic Joint. Here, as the previously analyzed SJ and RJ joints, constrains are implemented with the usage of **C** elements with some parameters to be tuned in order to get $\bar{\omega}_1^J = \bar{\omega}_2^J$, $v_{1x}^J = v_{2x}^J$ y $v_{1z}^J = v_{2z}^J$ for this special case. Then, for this kind of joint, only a displacement on the local y-axis direction between 1 and 2 extremes is allowed. The effort source **Se**=0 is introduced for this purpose, with a null force on the y-axis and both joint ends.

The transformation shown in Fig. 6 is similar to that presented above, in section 2.2, with the only difference that now, it is modulated, with the modulation factor (in this case r_y) that depends on the relative position between the joint extremes.

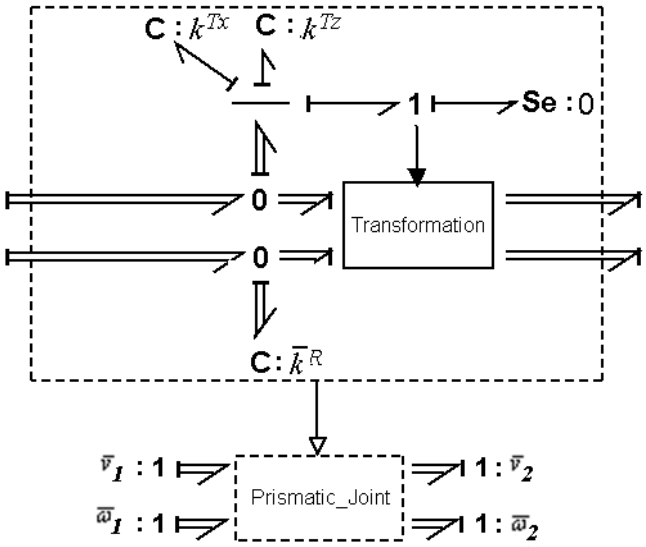

Fig. 6: Bond Graphs representation of the Prismatic Joint.

3 EXAMPLES AND SIMULATION RESULTS

In the following, three examples are presented involving mechanisms with three dimensional movements and different types of joints, modeled with the elements described in Section 2. The simulation model was developed in 20-Sim, and was validated against solutions obtained with the module Mecano of Samcef.

3.1 Example 1

Figure 7 show the physical description of first example and figure 8 the bond graph implementation of this example, which is built via assembling the previous submodels, pretty much in the same way as a real mechanism is constructed. This is due to the powerful graphical, modular and primarily acausal nature of bond graphs.

In order to model a mechanism, motion parts, mass properties, joints, geometrical properties and loads are created. The components for this example are two rigid bodies, a revolute joint J_1 and a spherical joint J_2. These components are parameterized with the following data: m_1 = 1Kg is the mass of the rigid body m_1; $I_{xx} = I_{yy} = I_{zz}$ = 4.167e-4 Kgm² are the principal moment of inertia of m_1; F_1 = -9.8 N is the weight of m_1; w = 0.5 rad/s is a speed of rotation imposed to (J_1); a = 0.3 m and b = 0.1 m are distances shown in figure 8.

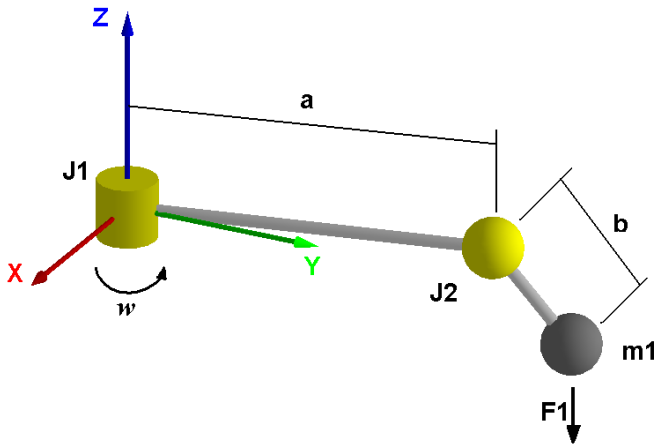

Fig. 7: Physic description of Example 1.

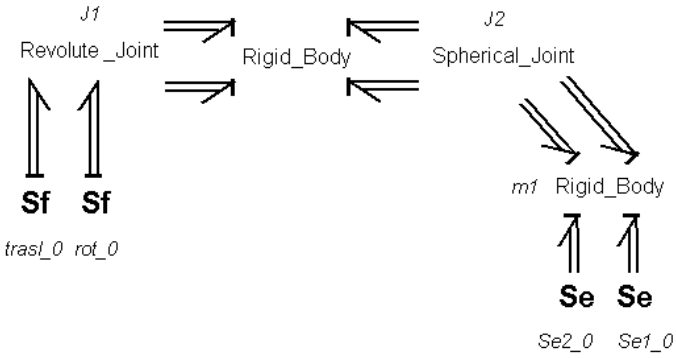

Fig. 8: Bond Graphs model of the example 1.

Figures 9, 10 and 11 show the rigid body m_1 g.c. position on axis X, Y, Z respectively vs. time. The results obtained from 20-Sim (blue) and Samcef (green) agree very well with no significant difference to be discussed.

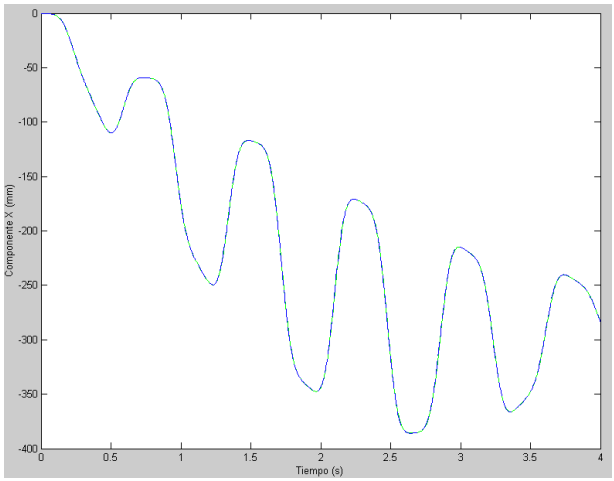

Fig. 9: Displacement global X-axis

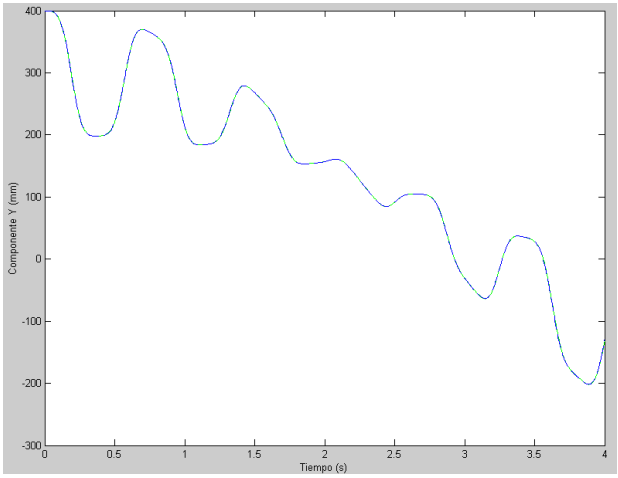

Fig. 10: Displacement global Y-axis

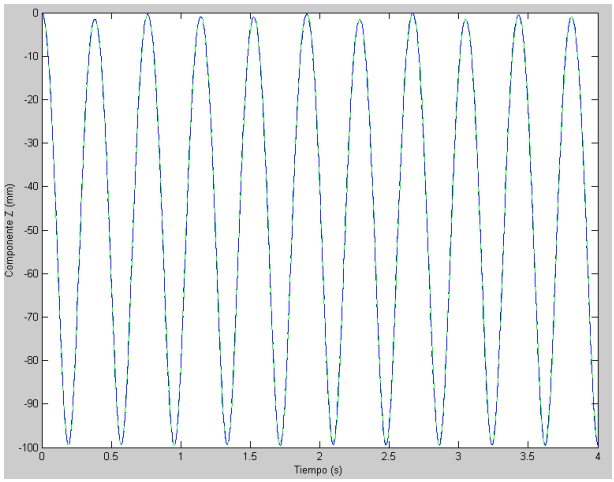

Fig. 11: Displacement global Z-axis

3.2 Example 2

Figure 12 show the physical description of the second example and figure 13 the bond graph implementation of this example. It is similar to example 1 but the spherical joint is replaced by a revolute joint (J_2) and is imposed a moment to J_1.

The components are parameterized with the following data: m_1 = 1Kg is the mass of the rigid body m; $I_{xx} = I_{yy} = I_{zz}$ = 4.167e-4 Kgm² are the principal moment of inertia of m; F = -9.8 N is the weight of m; M = 0.1 Nm is a moment imposed to J_1; a = 0.3m and b = 0.1m are distances shown in figure 12.

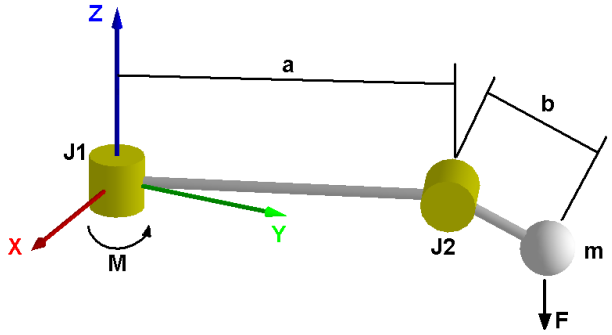

Fig. 12: Physic description of Example 2.

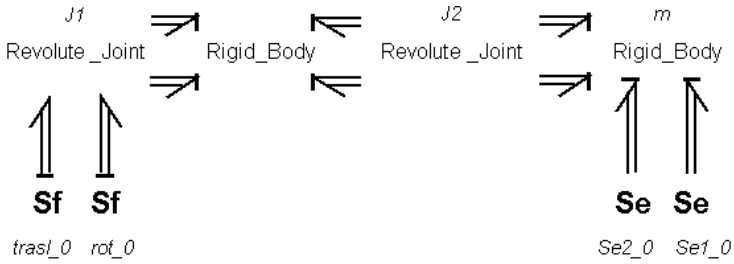

Fig. 13: Bond Graphs model of the example 2.

Figures 14, 15 and 16 show the rigid body m g.c. position on axis X, Y, Z respectively vs. time. The results obtained from 20-Sim (blue) and Samcef (green) agree very well with no significant difference to be discussed.

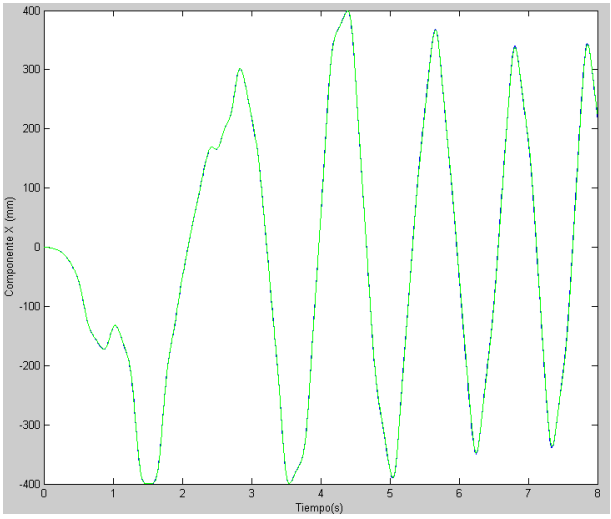

Fig. 14: Displacement global X-axis

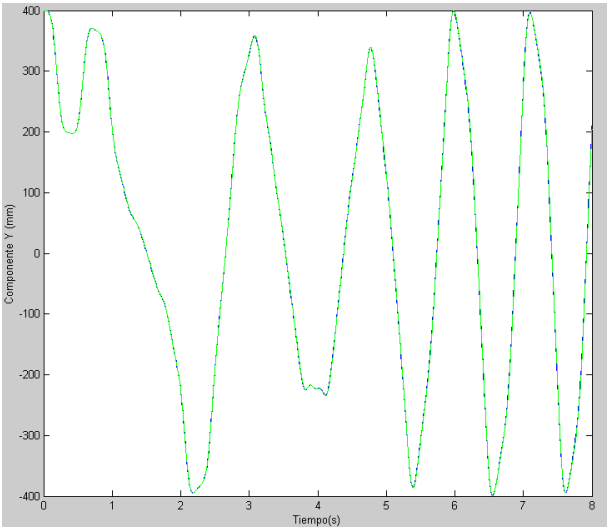

Fig. 15: Displacement global Y-axis

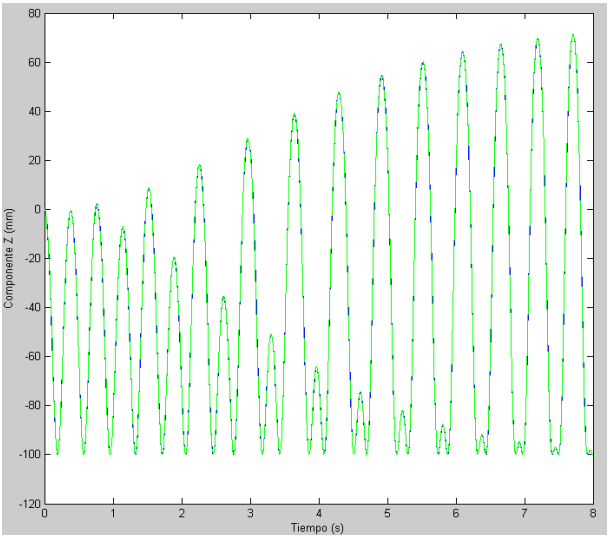

Fig. 16: Displacement global Z-axis

3.3 Example 3

Figure 17 shows the physical description of the third example and figure 18 the bond graph implementation of this example. It is similar to example 2 and it includes another rigid body, a prismatic joint (J_3) and a spring in the degree of freedom of this joint.

The components are parameterized with the following data: $m_1 = m_2 = 1$Kg are the mass of the rigid body m_1 and m_2; $I_{xx} = I_{yy} = I_{zz} = 4.167\text{e-}4$ Kgm² are the principal moment of inertia of m_1 and m_2; $F_1 = F_2 = -9.8$N are the weight of m_1 and m_2; $M = 0.1$ Nm is a moment imposed to (J_1); $K = 500$N/m is spring stiffness; $a = 0.3$m, $b = 0.1$m and $c_0 = 0.15$m are distances shown in figure 17.

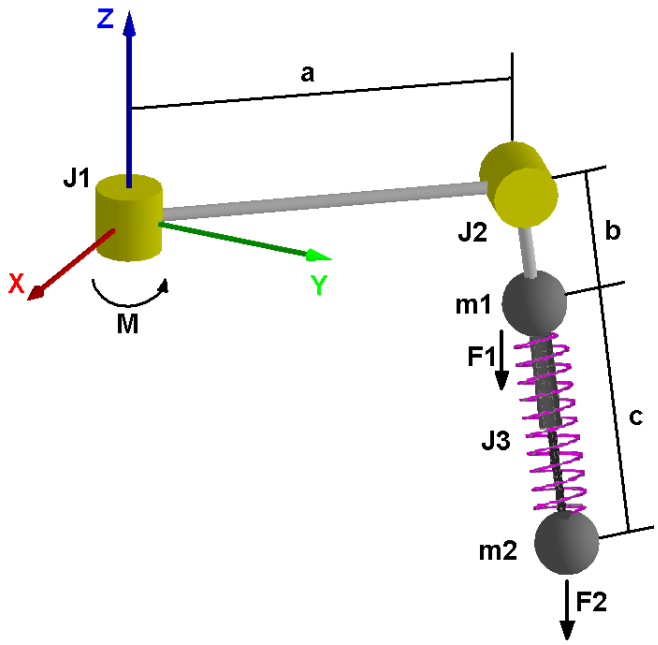

Fig. 17: Physic description of Example 3.

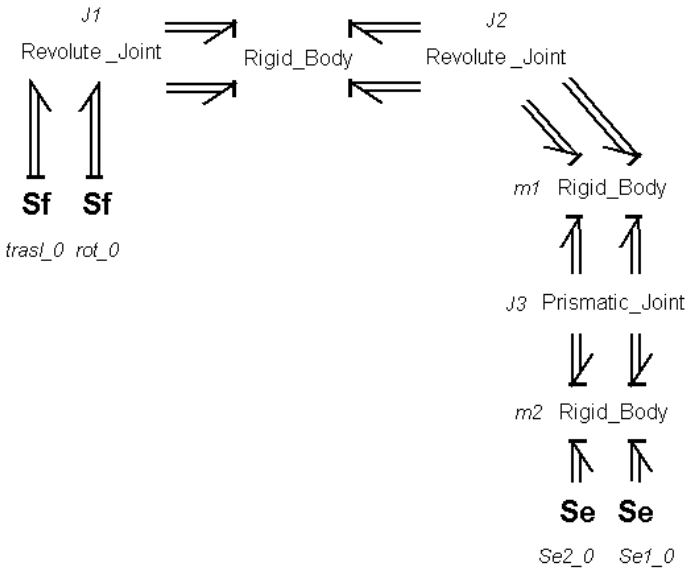

Fig. 18: Bond Graphs model of the Example 3.

Figures 19, 20 and 21 show again the rigid body m_2 g.c. position on axis X, Y, Z respectively vs. time. The results obtained from 20-Sim (blue) and Samcef (green) agree quite well, with some minor difference during the last part of the simulation that may be justified due to the difference between both time integrators.

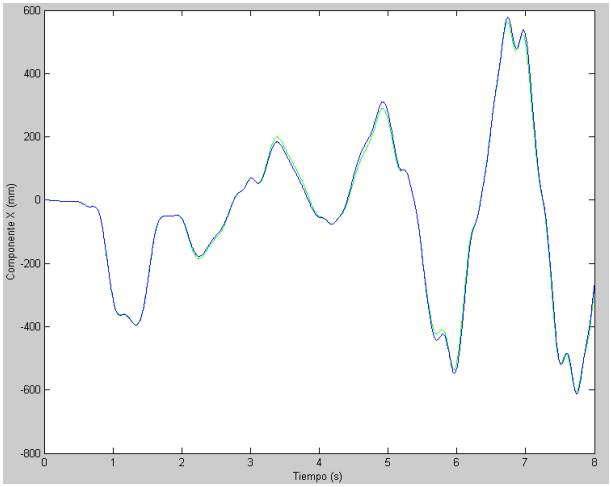

Fig. 19: Displacement global X-axis

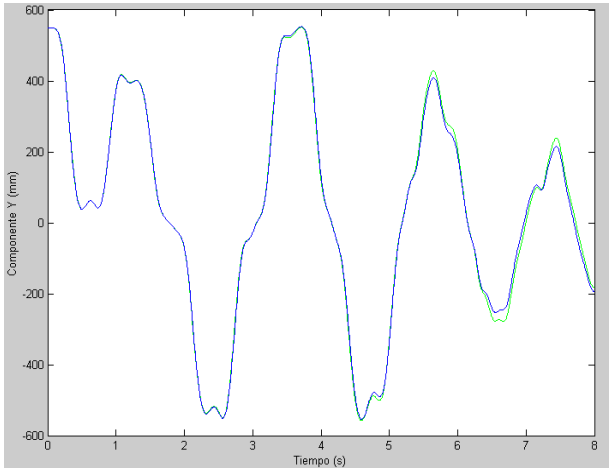

Fig. 20: Displacement global Y-axis

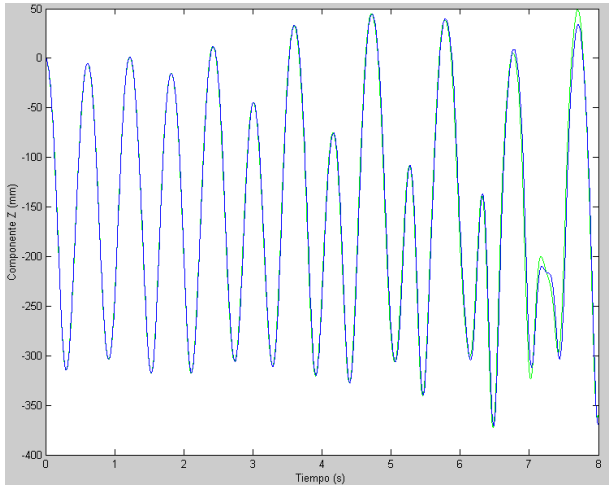

Fig. 21: Displacement global Z-axis

4 CONCLUSIONS

The main goal of this paper was the development of a multibond graph library for multibody systems focusing on an accurate representation of 3D large rotations. Several elements oriented to multibody systems were developed allowing to work with different reference frames, operating with them through the usage of translations and general transformations.

The graphical and primarily acausal nature of bond graphs allowed to develop a modular, hierarchical, object-oriented modeling tool for multibody systems which is well suited to the needs of practising engineers. Indeed, provided that the models of the system components exist in the library (being open it can be always extended to satisfy this requirement), all the modeler needs to do is to parameterize these submodels according to the physical and geometrical properties of each of the components and then assembly them according to the system configuration (given by the interconnection structure).

This library is currently being validated comparing its results against some equivalent solutions coming from other commercial software, in this case using Samcef. To start this validation, three examples were presented in this paper.

Some modules of this toolbox have been successfully used in vehicle modeling in order to predict dynamic behavior (Filippini (2004), Filippini et al. (2007)) and also were effectively applied to another project concerning vehicle fault diagnosis (Delarmelina et al. (2005)).

REFERENCES

Ronald C. Rosenberg, Donald L. Margolis, Dean C. Karnopp. Modeling and Simulation of Mechatronic Systems, *A Wiley-Interscience Publication*, New York.

Albert M. Bos. Modeling Multibody Systems in terms of Multibond Graphs, with application to a motorcycle, *PhD thesis at Twente Univ*. 1986

Ahmed A. Shabana. Dynamics of Multibody systems. *A Wiley-Interscience Publication*.

F. Cellier, "Hierachical non–linear bond graph: A unified methodology for modelling complex physical systems", *Simulation, Vol 58, No. 4*, pp. 230-248.

T. Ersal, J. Stein, L. Louca. A Bond Graph Based Modular Modeling Approach towards an Automated Modeling Environment for Reconfigurable Machine Tools. *IMAACA* 2004.

G. Filippini. Dinámica Vehicular mediante bond graphs. Proyecto final de carrera de grado. *Escuela de Ingeniería Mecánica*, Universidad Nacional de Rosario, 2004

G. Filippini, N. Nigro, S. Junco. Vehicle Dynamics Simulation using Bond Graphs. *IMAACA* 2007

D. Delarmelina, L. Silva, S. Junco. Fault Diagnosis in Vehicle based on its Dinamic Model. *Escuela de Ingeniería Mecánica y Escuela de Ingeniería Electronica*, Universidad Nacional de Rosario, 2005

Getting Started with 20-sim 3.6, Controllab Products B.V., Enschede, Netherlands. Internet: www.20sim.com, 2005.

M. Géradin, A. Cardona. Flexible Multibody Dynamics: A Finite Element Approach. John Wiley & Sons. 2001

SAMCEF User Manual V10.1. Internet: www.Samcef.com